Benzoate Cyclometalation Enables Oxidative Addition of Haloarenes at a Ru(II) Center

# Benzoate cyclometallation enables oxidative addition of haloarenes at a Ru(II) center

Marco Simonetti,[†] Rositha Kuniyil,[‡] Stuart A. Macgregor,[‡,*] Igor Larrosa[†,*]

[†] School of Chemistry, University of Manchester, Oxford Road, Manchester, M13 9PL, U.K.

[‡] Institute of Chemical Sciences, Heriot-Watt University, Edinburgh, EH14 4AS, U.K.

Supporting Information Placeholder

ABSTRACT: The first Ru(II)-catalyzed arylation of substrates without a directing group was recently developed. Remarkably, this process only worked in the presence of a benzoate additive, found to be crucial for the oxidative addition step at Ru(II). However, the exact mode of action of the benzoate was unknown. Herein, we disclose a mechanistic study that elucidates the key role of the benzoate salt in the C–H arylation of fluoroarenes with aryl halides. Through a combination of rationally designed stoichiometric experiments and DFT studies, we demonstrate that the aryl–Ru(II) species arising from initial C–H activation of the fluoroarene undergoes cyclometallation with the benzoate to generate an anionic Ru(II) intermediate. The enhanced lability of this intermediate, coupled with the electron-rich anionic Ru(II) metal center renders the oxidative addition of the aryl halide accessible. The role of an additional $(NMe_4)OC(CF_3)_3$ additive in facilitating the overall arylation process is also shown to be linked to a shift in the C–H pre-equilibrium associated with benzoate cyclometallation.
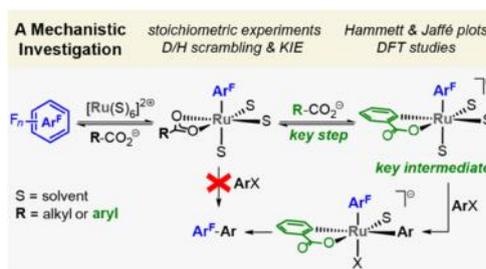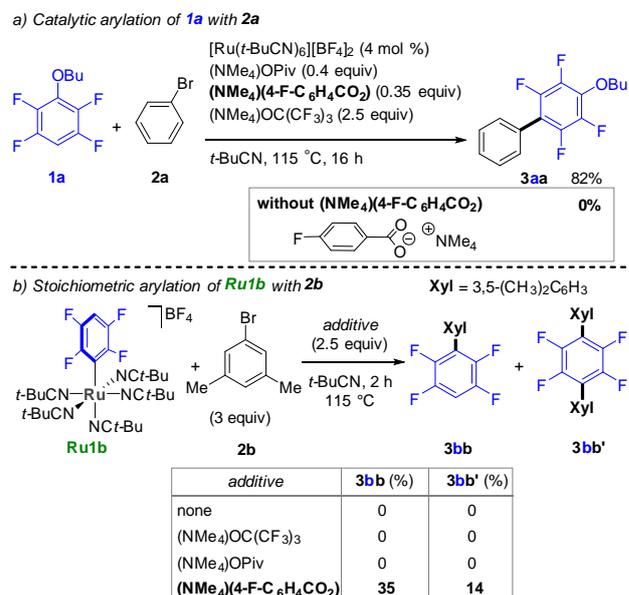
1. INTRODUCTION

The polyfluorobiphenyl unit is a recurrent building block found as a structural component in drugs,[1a-c] agrochemicals[1e,f] and numerous functional materials[1g-m] such as organic light-emitting diodes (OLEDs)[1j] and liquid crystals.[1k,i] Although cross-coupling methods can be applied to access these biaryl moieties,[2] C–H arylation strategies have been acknowledged as a more sustainable alternative strategy to selectively form aryl–aryl bonds.[3] In this context, fluorinated biaryls can be generated under Pd catalysis employing fluoroarenes with coupling partners such as aryl (pseudo)halides,[4a-d] aryl boronic donors,[4e] or simple arenes.[4f,g] Alternatively, Cu-[5] or Au-catalysts[6] can be used to promote analogous transformations. Recently, our group expanded upon the range of transition metal catalysts able to promote this particular type of coupling.[7] The arylation of fluoroarenes with aryl halides occurred with a Ru(II)-catalyst, $[Ru(t\text{-}BuCN)_6][BF_4]_2$, aided by $(NMe_4)OPiv$ and $(NMe_4)(4\text{-}F\text{-}C_6H_4CO_2)$ co-catalysts, and $(NMe_4)OC(CF_3)_3$ base in t-BuCN (Scheme 1a). Notably, this methodology is the first Ru-catalyzed C–H arylation process operating without the need for a directing group in the arene.

Crucially, this Ru-catalyzed C–H arylation only proceeded when a benzoate salt was present, with all other bases and carboxylates tested unable to switch on the reaction. Indeed, when the arylation of polyfluoroarene **1a** was carried out with bromobenzene **2a** under optimized reaction conditions in the absence of the benzoate additive, no cross-coupled product **3aa** was formed. To further clarify the surprising role of the benzoate source, a stoichiometric arylation between the catalytically active intermediate tetrafluorophenyl–Ru(II) complex **Ru1b** and 5-bromo-m-xylene **2b** was performed (Scheme 1b).

Biaryls **3bb** and **3bb'** were formed *only when the benzoate was added*. Remarkably, the structurally related pivalate salt did not promote the transformation. These empirical results, along with mechanistic studies and DFT calculations, led us to suggest a catalytic cycle where, although the initial C–H activation of the fluoroarene is assisted by pivalate, the formal

Scheme 1. The Importance of the Benzoate Additive in the Ru-Catalyzed Arylation of Fluorobenzenes

*a) Catalytic arylation of **1a** with **2a***

*b) Stoichiometric arylation of **Ru1b** with **2b***

| additive	3bb (%)	3bb' (%)
none	0	0
$(NMe_4)OC(CF_3)_3$	0	0
$(NMe_4)OPiv$	0	0
$(NMe_4)(4\text{-}F\text{-}C_6H_4CO_2)$	35	14

oxidative addition of the aryl halide could only proceed when benzoate was present.[7] However, the mechanism by which benzoate may facilitate oxidative addition remained unknown. Herein, we report mechanistic studies elucidating the role of the benzoate salt. Surprisingly, our experiments demonstrate that aryl–Ru(II) species such as **Ru1b**, which are inert towards oxidative addition with aryl bromides **2**, can undergo cyclometallation with the benzoate salt to form an anionic Ru(II)-intermediate that is highly reactive towards oxidative addition, and is essential to the reactivity of the system. In a similar vein, we have also recently proposed that the mechanism of the Ru(II)-catalyzed C–H arylation of *N*–chelating substrates with aryl (pseudo)halides involves an anionic bis-cyclometallated species as the key intermediate required for oxidative addition to occur.[8]

2. RESULTS AND DISCUSSION

2.1. Mechanistic hypothesis for the role of the benzoate. The specific requirement for a benzoate salt for the reaction to proceed led us to hypothesize that the benzoate may be undergoing *ortho*-C–H activation as its mode of action. Scheme 2 outlines our proposed catalytic cycle for the process. After the initial C–H activation of the fluoroarene **1** to form the cationic fluoroaryl–Ru(II) complex **II**, a second C–H activation event on the benzoate would generate anionic Ru(II)-species **IV** featuring a cyclometallated benzoate unit. This more electron-rich Ru(II) intermediate **IV** would be more reactive towards oxidative addition with the aryl halide (to **V**) than the cationic complex **II** or the neutral species **III**. Reductive elimination from **V** would then produce the biaryl product. In contrast, an aliphatic carboxylate such as pivalate would be unable to undergo cyclometallation and thus would be unable to promote the desired arylation reaction. Indeed, whereas the cyclometallation of aromatic benzoates by Ru(II) complexes is well-known and recognized,[9,10] the more challenging β-cyclometallation of aliphatic carboxylic acids has yet to be observed.

Scheme 2. Proposed Catalytic Cycle
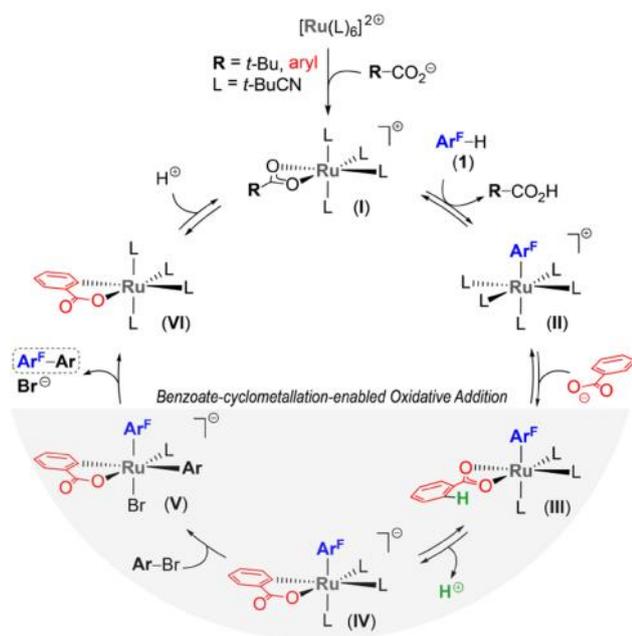
2.2. Kinetic and isotopic studies. With this mechanistic framework in mind, and given the possibility of isolating cationic intermediate **II**, we decided to examine stoichiometric arylation reactions to directly probe the cyclometallation and the oxidative addition steps without interference from the initial C–H activation of the fluoroarene (from **I** to **II**, Scheme 2). Thus, we started investigating the kinetic profile of the coupling of pentafluorophenyl–Ru(II) species **Ru1c** with bromoarene **2b** in the presence of a variety of benzoate derivatives (Figure 1). In order to standardize the measurements, **Ru1c** was pre-incubated for 20 min at 90 °C with the benzoate salt prior to the addition of **2b**. In agreement with our hypothesis, 2,6-disubstituted benzoate sources, which cannot undergo *ortho*-C–H activation, did not give any biaryl **3cb** irrespective of the electronic effect of these groups. Instead, paralleling our previous observations, $(NMe_4)(C_6H_5CO_2)$ triggered the desired coupling. In view of the often reversible nature of the C–H activation in Ru(II) catalysis,[11] we predicted that the addition of an external base would shift the equilibrium **III-IV** towards **IV** (Scheme 2), thus enhancing the reactivity. Indeed, when $(NMe_4)(C_6H_5CO_2)$ was used in combination with the base $(NMe_4)OC(CF_3)_3$, a conspicuous acceleration of the rate of arylation was obtained.[12] These data strongly suggest that the proposed *ortho*-metalation to generate intermediate **IV** is a key step *en route* towards the formation of the aryl–aryl bond.
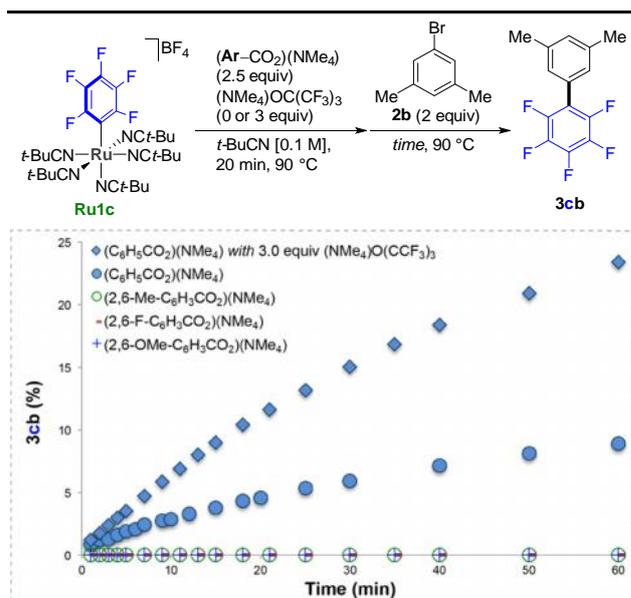
Figure 1. Stoichiometric arylation of **Ru1c** with **2b** employing (NMe_4)-2,6-disubstituted benzoates or simple benzoate in the presence or in the absence of $(NMe_4)OC(CF_3)_3$ base. Yield determined by GC-FID using hexadecane as internal standard.

In order to test this hypothesis further, catalytic arylation of non-volatile polyfluoroarene **1a** with bromoarene **2b** was carried out utilizing the deuterated $(NMe_4)(C_6D_5CO_2)$ under standard optimised reaction conditions[7] (Scheme 3). Analysis of the reaction mixture after 15 min revealed the formation of biaryl **3ab** in 16% yield. More importantly, recovered fluoroarene **1a**, showed 14% deuteration, and recovered benzoic acid revealed a 41% of H enrichment at the *ortho* positions. Since the only source of D was the benzoate salt, this experiment highlights the reversible nature of the steps from

Scheme 3. Catalytic Arylation of 1a with Bromoarene 2b Employing (NMe₄)C₆D₅CO₂ (Xyl = 3,5-dimethylphenyl).
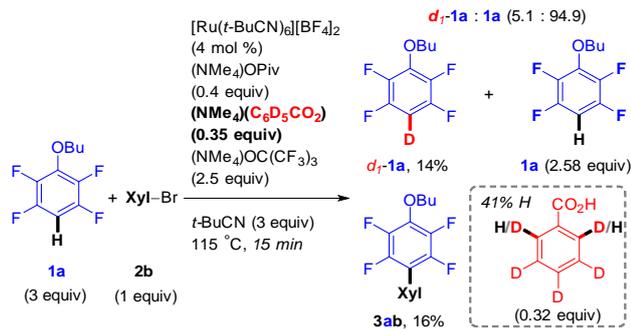
intermediate **I** to **IV** of the catalytic cycle (Scheme 2) and provides further evidence for the cyclometallation of the benzoic acid. Unfortunately, all attempts at isolation or *in situ* detection of **IV** starting from **Ru1c** in the presence of benzoate salts were unsuccessful, and this likely reflects the high energy of intermediate **IV** (see SI section 5 for details and DFT studies below).

Subsequently, we set out to investigate whether a KIE was associated with the benzoate cyclometallation step. The initial arylation rates of two independent stoichiometric couplings of pentafluorophenyl–containing **Ru1c** (intermediate **II** in Scheme 2) with 5-bromo-*m*-xylene **2b** using either (NMe₄)(C₆H₅CO₂) or (NMe₄)(C₆D₅CO₂) were therefore recorded (Figure 2). The rate of formation of biaryl **3cb** with the benzoate source was 1.36 faster than the one with the perdeuterated benzoic salt, suggesting that the cyclometallation of the benzoate (**III** to **IV** in Scheme 2) is kinetically relevant and likely an equilibrium under the reaction conditions.[13]
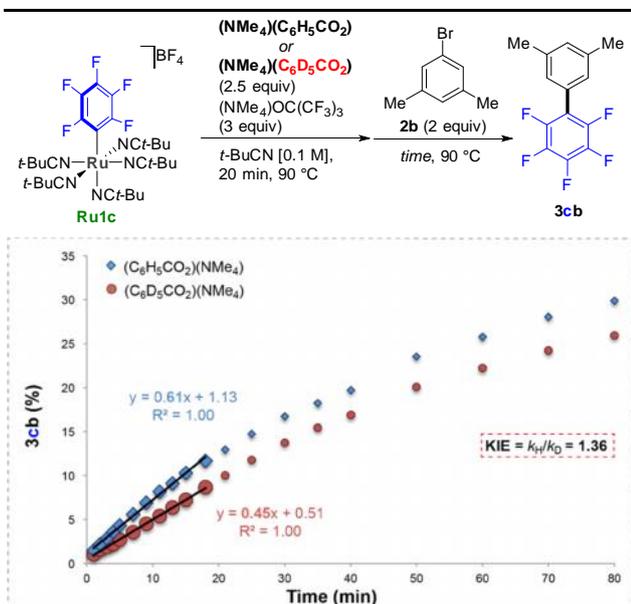
Figure 2. Stoichiometric arylation of **Ru1c** with **2b** employing (NMe₄)(C₆H₅CO₂) or (NMe₄)(C₆D₅CO₂) and (NMe₄)OC(CF₃)₃. Yield determined by GC-FID using hexadecane as internal standard.

2.3. Hammett and Jaffé Plots. In order to gain further mechanistic insights into the cyclometallation step of the benzoate additive, we compared the initial rates of formation of biaryl **3cb** in the stoichiometric arylation reactions of **Ru1c** with **2b** in the presence of a variety of electronically diverse 4-substituted benzoate salts (Table 1).[14] Firstly, and surprisingly, the rate of arylation (k_{obs}) increased with both electron-rich and electron-poor benzoates, with the parent unsubstituted benzoate displaying the slowest rate. A second observation from these data can be extracted from the corresponding Hammett plots (Figure 3).[15] While it is clear that most substituents fit well to a V-shaped Hammett plot (blue diamonds), there are four clear outliers (red circles and green triangles). From the constants of the groups studied, it can be seen that those highlighted in blue have similar σ_m and σ_p values. In contrast, the groups in red and green have significantly different values for their σ_m and σ_p constants. For example, the OMe and OEt groups have negative σ_p values (-0.27, -0.24) but positive σ_m (0.12, 0.10). These two groups show higher reactivity than would be expected from Figure 3, where only their σ_m or σ_p are considered in isolation. This implies that opposite electronic effects are synergistically combining to lower the overall $\Delta G^{\ddagger}$, thus enhancing the arylation rate. These observations suggest that both σ_m and σ_p must be considered at the same time. This is reasonable in the system under study as both the kinetically relevant cyclometallation (**III** to **IV**) and the rate-limiting aryl bromide oxidative addition (**IV** to **V**) steps may be affected by electronic perturbation at the *meta* and *para* sites of the benzoate substrates (C$_{Ar}$–H (σ_m), C(O)O⁻/H (σ_p), C$_{Ar}$–[Ru] (σ_m), C(O)O–[Ru] (σ_p),) at several points in the

Table 1. Hammett Plots: Initial Rates Data of the Arylation of Ru1c with Bromoarene 2b employing different 4-Substituted Benzoates.

| Entry		σ_m	σ_p	k_{obs} (%/min)	log (k/k_0)
1	NMe₂	-0.16	-0.83	1.7334	0.4906
2	*t*-Bu	-0.10	-0.20	0.7858	0.1470
3	Me	-0.07	-0.17	0.7283	0.1140
4	H	0	0	0.5602	0
5	CH₂CN	0.16	0.18	1.0770	0.2839
6	C₆F₅	0.26	0.27	1.8236	0.5126
7	OCF₃	0.38	0.35	2.5290	0.6546
8	CF₃	0.43	0.54	2.7943	0.6979
9	OMe	0.12	-0.27	1.7610	0.4974
10	OEt	0.10	-0.24	1.5220	0.4341
11	OPh	0.25	-0.03	2.4571	0.6411
12	F	0.34	0.06	1.7222	0.4877

Stoichiometric arylation of **Ru1c** with **2b** employing *para*-substituted (NMe₄)-benzoates and (NMe₄)OC(CF₃)₃ base. Initial arylation rates in formation of **3cb** were determined by GC-FID using hexadecane as internal standard.

Hammett equation:
$$\log\left(\frac{k_X}{k_H}\right) = \rho_m\sigma_n + \rho_p\sigma_p \qquad (1)$$

if $\sigma_n \cong \sigma_p \Rightarrow \log\left(\frac{k_X}{k_H}\right) = \rho_n\sigma_n + \rho_p\sigma_n = (\rho_n + \rho_p)\sigma_n \quad (2)$

if $\sigma_p \cong \sigma_n \Rightarrow \log\left(\frac{k_X}{k_H}\right) = \rho_n\sigma_p + \rho_p\sigma_p = (\rho_n + \rho_p)\sigma_p \quad (3)$
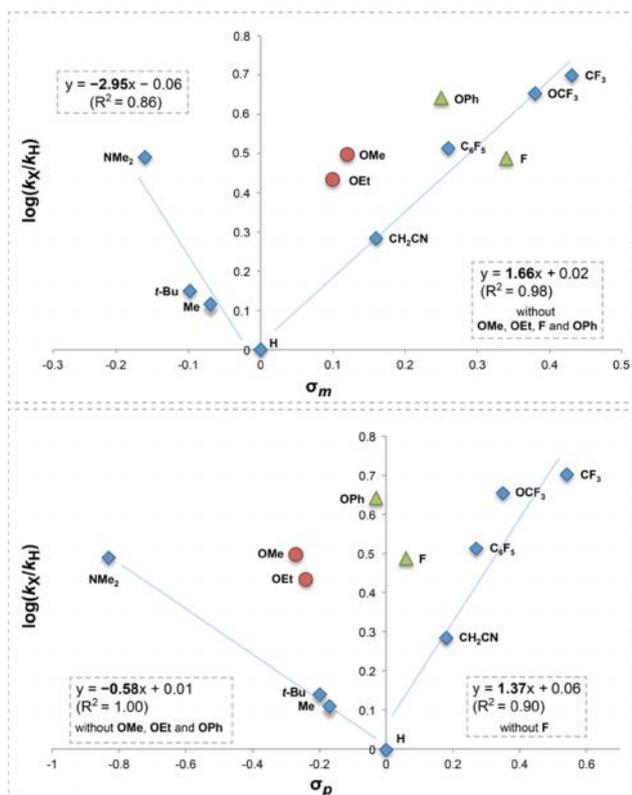

Figure 3. Evaluation of benzoate electronic effect on rate. Hammett plots: $\log(k_X/k_H)$ vs σ_m (top) and σ_p (bottom).

arylation process (Figure 4). We return to deconvolute these *meta* and the *para* effects in the computational section below. Indeed, considering the Hammett equation 1, a Hammett plot should only result in a linear relationship if the electronic influence of the R group affects only one position of the aromatic (*meta* or *para*) of a kinetically relevant step (i.e., if $\rho_p\sigma_p \gg \rho_m\sigma_m$ or $\rho_m\sigma_m \gg \rho_p\sigma_p$). However, excluding the groups with significantly different σ_m vs σ_p (OMe, OEt, OPh and F), a linear free energy relationship (LFER) based on Hammett equations 2 and 3 could be seen (Figure 3, blue diamonds). The higher absolute values of the two ($\rho_m+\rho_p$) values for both electron-donating and electron-withdrawing groups observed in the *meta* V-shaped Hammett plot of equation 2
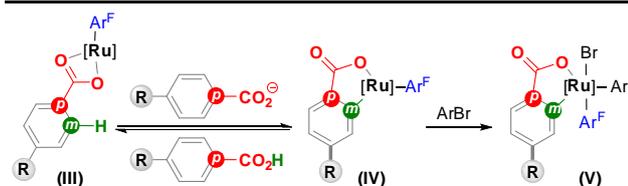

Figure 4. The influence of the R group on the electronic properties at multiple *meta* and *para* positions affecting the kinetically relevant cyclometallation, as well as the oxidative addition step.

(($\rho_m+\rho_p$)^{EDG}= -2.95; ($\rho_m+\rho_p$)^{EwG}= 1.66), indicate that, while both are important, the electronic perturbation at the C_{Ar}–[Ru]/C_{Ar}–H sites has a greater impact on the overall rate than that at C(O)O–[Ru]/C(O)O$^-$/H (*para* V-shaped Hammett plot of equation 3; ($\rho_m+\rho_p$)^{EDG}= -0.58; ($\rho_m+\rho_p$)^{EwG}= 1.37).

Although V-shaped Hammett plots are usually associated with a change in the mechanism of the process,[16] the lowering of the overall $\Delta G^\ddagger$ due to a weighed variation of the electronic properties of the *meta* and *para* positions of the benzoates associated with the kinetically relevant cyclometallation, provides a more logical explanation for our experimental data (see also the DFT studies below). To validate further this hypothesis, we applied to our system Jaffé's extension of the Hammett equation. This modification allows the correlation of substituent perturbations that influence more than one reactive center at the same time to be plotted (Figure 5).[17] In the Jaffé equation, the Hammett equation is divided by one of the two σ values. Depending on which σ constant is in the denominator, the slope of the plot gives one ρ value, while the y-intercept provides the other ρ value (equations 4 and 5). In order to verify the LFER, both plots should result in the same values of ρ_m and ρ_p. As shown in Figure 5, this treatment of the data led to two plots showing a LFER valid for *all* the substituents. Similar ρ values were obtained in both cases ($\rho_m \cong 2.2$; $\rho_p \cong -1.2$),

Jaffé equation:
$$\frac{\log\left(\frac{k_X}{k_H}\right)}{\sigma_n} = \frac{\rho_F\sigma_p}{\sigma_n} + \rho_n \qquad (4)$$
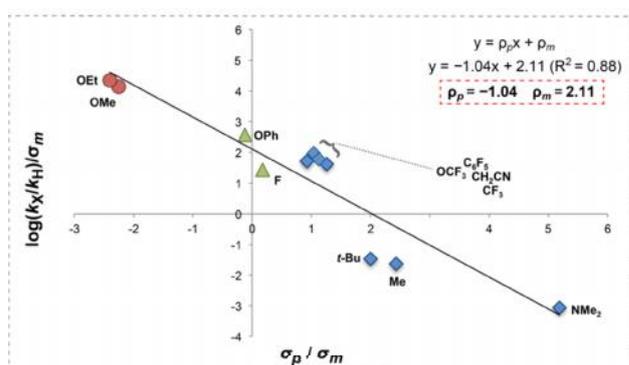
Jaffé equation:
$$\frac{\log\left(\frac{k_X}{k_H}\right)}{\sigma_p} = \frac{\rho_m\sigma_n}{\sigma_p} + \rho_p \qquad (5)$$
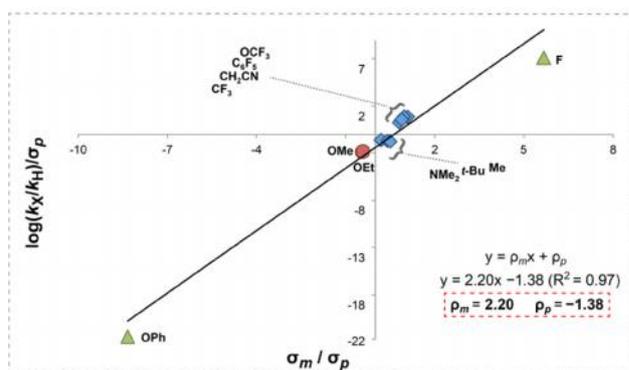

Figure 5. Jaffé plots displaying a linear free energy relationship between the benzoate source and the reaction rate ($\rho_m \cong 2.2$; $\rho_p \cong -1.2$).

thus validating our mechanistic framework and confirming the greater magnitude of the electronic perturbation on the C_{Ar}–H/[Ru]–C_{Ar} bonds on the overall rate. Finally, the signs of ρ_m and ρ_p indicate that the overall rate is enhanced by placing EDGs at *para* and EWGs at *meta* positions, which is consistent with the observation that OMe and OEt substituents are visibly outliers in both V-shaped Hammett plots. Importantly, as the *meta* effect is more significant than the *para* one, it should also be noted that in the *para* V-shaped Hammett plot both OPh and F significantly deviate from linearity, as both rates are largely overestimated due to the greater contribution of the *meta* effect. Instead in the *meta* V-shaped Hammett plot OPh and F are marginally over- and underestimated, respectively. Although both substituents have positive ρ_m (F= 0.34, OPh= 0.25), OPh has a slightly negative ρ_p (-0.03), while F has a slightly positive one (0.06), which explains why OPh lies above, and F below, the linear fitting.

2.4. DFT Studies. We have also probed the mechanism of these benzoate-assisted arylation reactions with density functional theory (DFT) calculations. The reaction of a model system, $[Ru(C_6F_5)(MeCN)_5]^+$ (denoted **II'**), with PhBr in the presence of $PhCO_2^-$ was considered, with all geometries optimized with the BP86 functional using a modest basis set (BS1, see Computational Details, ESI). Energies were then recomputed using the ωB97X-D functional with a def2-TZVP basis set and incorporating MeCN solvation via a PCM correction. Test calculations indicated the use of MeCN in place of the *t*-BuCN ligands had little effect on the overall profile, with most stationary points being destabilized by 2-4 kcal/mol (see Figure S21, ESI). Figure 6 summarizes the most accessible computed free energy profile based on the proposed catalytic cycle in Scheme 2. For each step alternative geometric isomers were assessed and details are supplied in the ESI (Figures S3-S7). Intermediates involved in ligand exchange steps are omitted here for clarity but are considered in the kinetic modeling (see below, Figure 9(a)). Starting with $[Ru(C_6F_5)(MeCN)_5]^+$, **II'**, exchange of two MeCN ligands with $PhCO_2^-$ yields *mer*-$[Ru(C_6F_5)(MeCN)_3(\kappa^2-PhCO_2)]$, ***mer*-III'**, which, at -5.57 kcal/mol, proves to be the most stable intermediate prior to the C–H and C–Br bond activation events. Further MeCN/$PhCO_2^-$ substitution forms $[Ru(C_6F_5)(MeCN)_2(\kappa^1-PhCO_2)(\kappa^2-PhCO_2)]^-$
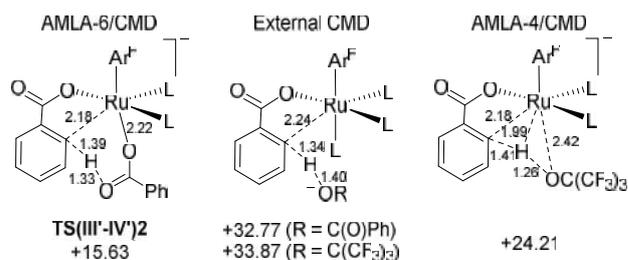
Figure 7. Geometries of alternative C–H activation transition states with selected key distances in Å and relative free energies in kcal/mol (L = MeCN, $Ar^F = C_6F_5$). Geometric data for the external CMD transition state are for R = C(O)Ph; see ESI for more details and alternative isomers (Figures S8 and S9).

Int(III'-IV')1 at -4.57 kcal/mol. This species then undergoes a 2-step C–H activation via agostic intermediate **Int(III'-IV')2** at +4.53 kcal/mol from which C–H bond cleavage proceeds via an AMLA-6/CMD transition state (ambiphilic metal-ligand assistance/concerted metalation deprotonation),[18] **TS(III'-IV')2**, at +15.63 kcal/mol (see also Figure 7 for geometric details). This gives a cyclometallated species **Int(III'-IV')3** at +9.90 kcal/mol as a benzoic acid adduct. $PhCO_2H$/MeCN substitution then forms ***fac*-IV'** at +9.62 kcal/mol.[19] The overall barrier to C–H activation is 21.20 kcal/mol and the formation of ***fac*-IV'** is endergonic by 15.19 kcal/mol.

Alternative C–H bond activation mechanisms were also assessed and shown to be energetically less accessible (Figure 7). Thus transition states for external CMD at $[Ru(C_6F_5)(MeCN)_3(\kappa^1-PhCO_2)]$ by $PhCO_2^-$ lie above 30 kcal/mol. A direct role for $^-OC(CF_3)_3$ as a base in C–H activation was also ruled out, either as an external CMD process, or as an intramolecular base (AMLA-4/CMD). We return to the role of $^-OC(CF_3)_3$ in promoting the arylation reaction below.

PhBr activation at ***fac*-IV'** requires initial MeCN substitution and, in principle, could occur at 6-coordinate $[Ru(C_6F_5)(MeCN)_2(\kappa-C,O-C_6H_4CO_2)(PhBr)]^-$, either as a concerted oxidative addition to yield 18e⁻ Ru(IV) $[Ru(C_6F_5)(MeCN)_2(\kappa-C,O-C_6H_4CO_2)(Ph)(Br)]^-$, or via
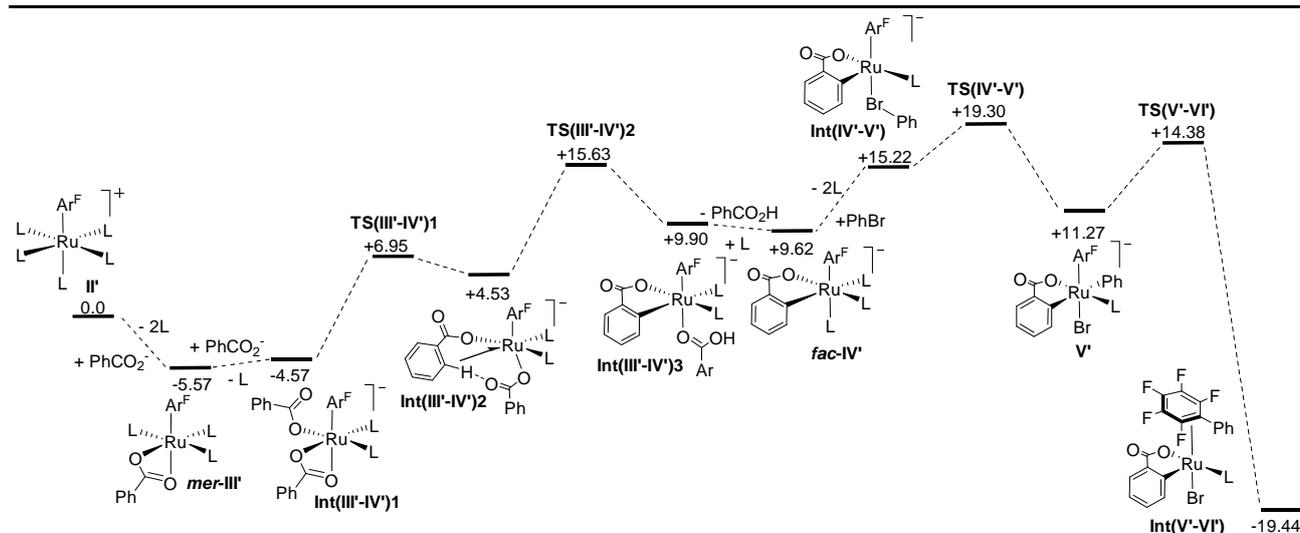
Figure 6. Computed free energy reaction profile (ωB97X-D(BS2, acetonitrile)//BP86, L = MeCN, $Ar^F = C_6F_5$, kcal/mol) for the arylation of C_6F_5H with PhBr starting from model intermediate $[Ru(C_6F_5)(MeCN)_5]^+$, **II'**.

nucleophilic displacement of Br⁻ to form 16e⁻ Ru(C₆F₅)(MeCN)₂(κ-*C,O*-C₆H₄CO₂)(Ph)] (see Figure 8 and Figures S10-S11). Such processes, however, proved to have very large barriers. Instead a second MeCN ligand is lost to form square-pyramidal [Ru(C₆F₅)(MeCN)(κ-*C,O*-C₆H₄CO₂)(κ-*Br*-PhBr)]⁻, **Int(IV'-V')**. This species has 12 possible geometric isomers of which 11 proved to be local minima (see Figure S7); the lowest energy form is shown in Figure 6 and benefits from having the strong donor aryl ligand in the axial position as well as the weak PhBr ligand opposite the high *trans* influence C₆F₅. PhBr is computed to prefer binding through the Br substituent over alternative η²-C₆H₅Br forms and IRC calculations subsequently confirmed that this Br-bound intermediate lies directly on the pathway for concerted oxidative addition. This proceeds via **TS(IV'-V')** at 19.30 kcal/mol to give **V'** at +11.27 kcal/mol. Ph–C₆F₅ reductive coupling then readily occurs via **TS(V'-VI')** at +14.38
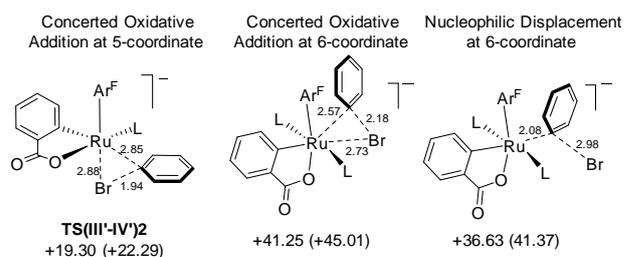

Figure 8. Geometries of alternative C–Br activation transition states with selected key distances in Å and relative free energies in kcal/mol (L = MeCN, Arᶠ = C₆F₅). Examples shown are the lowest energy transition states located for each process; full details of isomers are in the ESI (Figures S10 and S11). Data in parenthesis are for optimizations including a PCM correction for acetonitrile solvent.
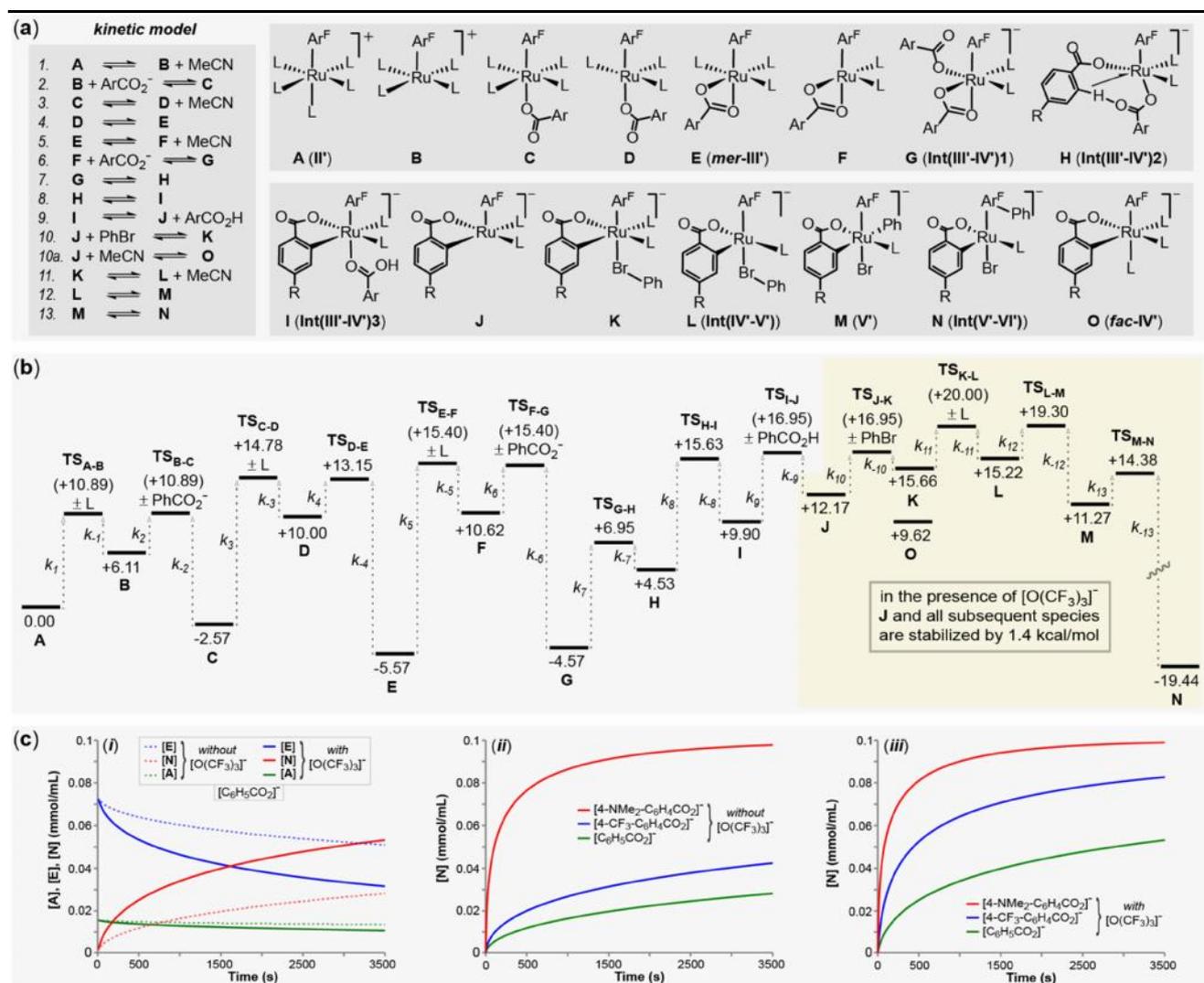
Figure 9. (a) Kinetic model for the reaction of **II'** (denoted **A** in the kinetic model) with PhBr in the presence of benzoates 4-R-C₆H₄CO₂⁻ to give **Int(V'-VI')** (denoted **N**; L = MeCN, Arᶠ = C₆F₅). Ligand addition steps are assumed to proceed at the diffusion-controlled limit and are indicated by TS energies shown in parentheses. (b) Computed reaction profile (kcal/mol) with PhCO₂⁻ highlighting the effect of the ⁻OC(CF₃)₃ additive; see Figure S13 for equivalent diagrams computed with 4-NMe₂-C₆H₄CO₂⁻ and 4-CF₃-C₆H₄CO₂⁻. (c) Computed kinetic profiles at 363 K comparing arylation (*i*) in the presence of PhCO₂⁻, with and without the ⁻OC(CF₃)₃ additive, (*ii*) in the presence of benzoates 4-R-C₆H₄CO₂⁻ (R = H, NMe₂ and CF₃) without ⁻OC(CF₃)₃, and (*iii*) in the presence of benzoates 4-R-C₆H₄CO₂⁻ (R = H, NMe₂ and CF₃) with added ⁻OC(CF₃)₃.

kcal/mol and gives **Int(V'-VI')** (-19.44 kcal/mol) in which the biaryl product is bound in an η^2-fashion to Ru.[20]

The free energy profile for arylation in Figure 6 indicates that the overall rate-limiting process is associated with C–Br activation via **TS(IV'-V')** at +19.30 kcal/mol and that this corresponds to an overall barrier of 24.87 kcal/mol. C–H activation is therefore a pre-equilibrium, the endergonic nature of which is consistent with reversible C–H activation leading to H/D exchange at the *ortho* position and a modest (equilibrium) kinetic isotope effect.

As discussed above and shown in Figure 7, the role of the $^-$OC(CF$_3$)$_3$ additive in promoting arylation cannot be ascribed to any direct participation in the C–H activation event. Instead we postulate that $^-$OC(CF$_3$)$_3$ affects the position of the C–H activation pre-equilibrium via deprotonation of the benzoic acid produced in this process. Based on the pK_a values of PhCO$_2$H and HOC(CF$_3$)$_3$ in water (4.2 and 5.2 respectively) this implies a free energy change of -1.4 kcal/mol upon deprotonation. To quantify this effect a kinetic model accommodating all the steps linking **II'** to **Int(V'-VI')** was constructed (see Figure 9(a)) where any ligand substitution processes were treated as dissociative in nature with the ligand addition steps assumed to occur at the diffusion-controlled limit ($k = 10^{10}$ M^{-1}s^{-1}, corresponding to a barrier of 4.78 kcal/mol at 363 K). This allows for the rate of the related ligand dissociation to be defined, based on the equilibrium constant computed for the overall ligand exchange. Within this model $^-$OC(CF$_3$)$_3$ intervenes upon loss of PhCO$_2$H from species **I** and its effect is modelled by a 1.4 kcal/mol stabilization of all species from **J** onwards (right-hand shaded area, Figure 9(b)). This leaves the rates of the onward reactions unchanged, but reduces the rate of the backwards reaction (i.e. **J** + PhCO$_2$H → **I**). The effect is seen in Figure 9(c), plot (*i*) which shows that product formation (modelled by species **N**) is approximately doubled over a 1 h period in the presence of the $^-$OC(CF$_3$)$_3$ additive (compare the dotted and solid red lines). This is in good agreement with experimental observations which indicate a ca. 3-fold rate enhancement (Figure 1).

The profile in Figure 9(b) was recomputed with two substituted benzoates, 4-R-C$_6$H$_4$CO$_2^-$, with R = NMe$_2$ and CF$_3$. These substituents have distinctly different σ_p and σ_m Hammett parameters, yet experimentally both provide significantly enhanced reactivity compared to the parent benzoate (Table 1). In each case a similar overall profile was computed, with the transition state for C–Br activation lying above that for C–H activation (see Table 2 and Figures S12-13). The results again emphasize the sensitivity of the overall outcome to the inclusion of the $^-$OC(CF$_3$)$_3$ additive in the model. This is more apparent for 4-CF$_3$-C$_6$H$_4$CO$_2^-$ for which a reduction of 2.16 kcal/mol in ΔG_{CHA} leads to an order of magnitude reduction in the computed t$_{1/2}$, the time required to reach 50% conversion. The higher pK_a of 4-NMe$_2$-C$_6$H$_4$CO$_2$H means the effect here is less dramatic, but in this case the computed barrier in the absence of $^-$OC(CF$_3$)$_3$ is already significantly lower than the PhCO$_2^-$/$^-$OC(CF$_3$)$_3$ system.

The data in Table 2 indicate that the overall barrier to arylation ($\Delta G^{\ddagger}_{span}$) depends more on the free energy change of the C–H activation (ΔG_{CHA}) rather than the subsequent barrier to PhBr activation ($\Delta G^{\ddagger}_{PhBr}$). The variation in ΔG_{CHA} is mirrored in the trend in the 2-step C–H activation (**G→I**: R = NMe$_2$ (+12.23 kcal/mol) < R = CF$_3$ (+13.74 kcal/mol) < R = H (14.47 kcal/mol)). The fact that both an electron-donating and an electron withdrawing substituent reduce the barrier to C–H

Table 2. Selected computed data (kcal/mol unless otherwise stated) for the arylation reaction with different benzoates 4-R-C$_6$H$_4$CO$_2^-$.[a,b]

Ⓡ	$^-$OC(CF$_3$)$_3$	$\Delta G^{\ddagger}_{CHA}$	ΔG_{CHA}	$\Delta G^{\ddagger}_{PhBr}$	$\Delta G^{\ddagger}_{span}$	t$_{1/2}$ (s)
H	N	21.20	+17.74	7.13	24.87	18102
	Y		+16.34		23.40	2954
NMe$_2$	N	19.77	+13.93	7.32	21.25	106
	Y		+13.65		20.97	81
CF$_3$	N	19.84	+16.15	7.61	23.76	6084
	Y		+14.19		21.80	446

[a]Definitions: $\Delta G^{\ddagger}_{CHA} = \Delta G(\mathbf{TS_{H-I}} - \mathbf{E})$; $\Delta G_{CHA} = \Delta G(\mathbf{J} - \mathbf{E})$; $\Delta G^{\ddagger}_{PhBr} = \Delta G(\mathbf{TS_{L-M}} - \mathbf{J})$; $\Delta G^{\ddagger}_{span} = \Delta G(\mathbf{TS_{L-M}} - \mathbf{E})$;[21] t$_{1/2}$ = time to 50% conversion. See Figure 9 for labels of stationary points. [b]Corrections for the effect of $^-$OC(CF$_3$)$_3$ are based on the pK_as of HOC(CF$_3$)$_3$ (5.2) and PhCO$_2$H (4.2) in water; pK_as for the 4-R-C$_6$H$_4$CO$_2$H acids (R = NMe$_2$: 5.03; R = CF$_3$: 3.66) are based on the difference in the σ_p Hammett parameters and the relationship $\sigma = -($pK_a(4-R-C$_6$H$_4$CO$_2$H) $-$ pK_a(PhCO$_2$H)).

activation over the unsubstituted parent has parallels in the trends computed by Gorelsky and Fagnou for C–H activation of (hetero)aromatics at Pd(Ph)(OAc)(PMe$_3$),[4d,22] although the variations are much smaller here. The effect of the $^-$OC(CF$_3$)$_3$ base is also a significant factor in accelerating the reaction, especially with the 4-CF$_3$-C$_6$H$_4$CO$_2^-$ additive.

As highlighted in Figure 4 electronic perturbation arising from the benzoate substituent, R, could manifest itself at several points along the reaction pathway. The initial cyclometallation involves C$_{Ar}$–H bond cleavage and formation of a C$_{Ar}$–[Ru] bond, both of which should be sensitive to σ_m; similarly this process involves varying the C(O)O–[Ru] interaction and H$^+$ transfer to a second benzoate to form a C(O)O–H bond which will be more dependent on σ_p. As discussed above the the C–Br activation step shows little dependency on R and so we have focused on deconvoluting how σ_m and σ_p affect ΔG_{CHA}.

To this end we have computed the free energy changes for the model cyclometallation processes (4) and (5) for all the 4-R-C$_6$H$_4$CO$_2^-$ substrates studied experimentally (see Figure 10). In (4) cyclometallation of the parent benzoate in **E** proceeds with different 4-R-C$_6$H$_4$CO$_2^-$ acting as the base: ΔG(4) should therefore reflect how σ_p promotes C–H activation. In (5) the cyclometallation of different 4-R-C$_6$H$_4$CO$_2^-$ in **E** proceeds with the parent benzoate acting as the base. ΔG(5) should be dominated by the breaking of the C$_{Ar}$–H bond and the formation of the new [Ru]–C$_{Ar}$ bond, and as such, should correlate with σ_m. However, σ_p may also play a role here by influencing how the C(O)O–[Ru] interaction varies due to the κ^2-κ^1 change in substrate binding mode. This point was considered in process (6) and was found to be favored by electron-donating *para*-substituents. This effect is relatively weak, however, with a plot of ΔG(6) vs. σ_p giving a straight line of gradient 2.1 (R^2 = 0.92, see Figure SX).

Plots of ΔG(4) *vs.* σ_p and ΔG(5) *vs.* σ_m are displayed in Figure 10. In both cases a good correlation is found; moreover the plots provide further evidence for the counter-balancing effects of the *para*- and *meta*-substituents. Thus the cyclometallation is facilitated by electron donating *para*-substituents which enhance substrate basicity (ΔG(4) *vs.* σ_p) while for a given base substrate cyclometallation is favored by electron-withdrawing *meta*-substituents (ΔG(5) *vs.* σ_m).[23] Importantly,
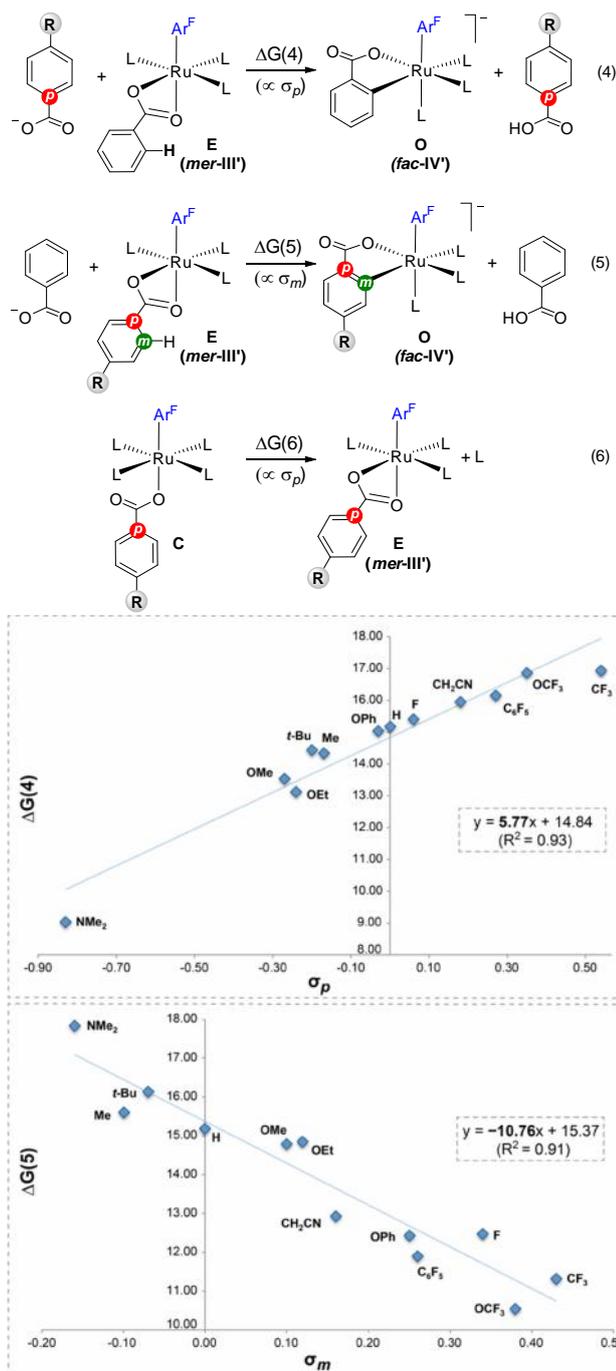
Figure 10. Model reactions considered to isolate σ_p and σ_m effects and the resultant plots of $\Delta G(4)$ *vs.* σ_p and $\Delta G(5)$ *vs.* σ_m.

the gradients indicate the latter *meta*-effect is approximately twice as large as the former *para*-effect, in excellent agreement with the conclusions from the Jaffé plots in Figure 5.

The trend in the *meta* effect as defined in process (5) must relate to differences in the C_{Ar}–H and [Ru]–C_{Ar} bond energies. Direct computation of the C_{Ar}–H homolytic bond dissociation energies shows little variation as a function of R, with most benzoates giving a value of 102 ± 0.5 kcal/mol (see ESI, Table S5). The [Ru]–C_{Ar} bond strength must therefore dominate, with these being stronger with electron-withdrawing substituents. There is precedent for this in the selective C–H of fluoroarenes,[24] and in M–C bond strengths being more sensi-

tive to substituent effects than their equivalent C–H bonds.[25]

2.5 The role of benzoate cyclometallation in promoting arylation. Although the C–Br activation step proving insensitive to substituent effects on the benzoate, cyclometallation remains the key to making the overall arylation process accessible. To understand this more fully, C–Br activation was modelled at cationic, neutral and non-cyclometallated anionic analogues of **L**/**Int(IV'-V')** and the most accessible processes for each case are shown in Figure 11. The data show two trends when moving from cationic through neutral and then to anionic systems: (i) the 5-coordinate precursor to C–Br activation becomes more accessible and (ii) the subsequent barrier to C–Br activation is reduced. Both factors make the overall barriers at $[Ru(C_6F_5)(MeCN)_3(PhBr)]^+$ and neutral $[Ru(C_6F_5)(MeCN)_2(\kappa^2\text{-PhCO}_2)(PhBr)]$ prohibitively high. This is still the case for $[Ru(C_6F_5)(MeCN)(\kappa^1\text{-PhCO}_2)_2(PhBr)]^-$,[26] although interestingly for $[Ru(C_6F_5)(\kappa^2\text{-PhCO}_2)(\kappa^1\text{-PhCO}_2)_2(PhBr)]^-$ the barrier to C–Br activation falls to only 3.97 kcal/mol. This is in fact slightly lower than the barrier from cyclometallated **L** (4.08 kcal/mol), although in this case the low energy of **L** (+15.22 kcal/mol) allows C–Br activation to proceed via $\mathbf{TS_{L-M}}$/**TS(IV'-V')** at only +19.30 kcal/mol. The role of the cyclometallated benzoate is therefore not just to enhance the electron-rich character of the Ru(II) center, but
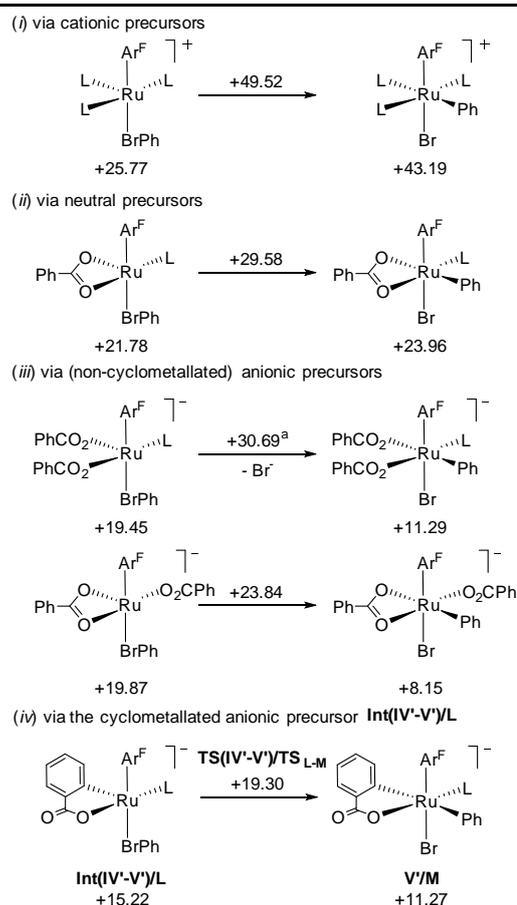

Figure 11. Lowest energy pathways (kcal/mol, L = MeCN, $Ar^F = C_6F_5$) computed for C–Br activation at 5-coordinate cationic, neutral and anionic precursors, placing the Ph group *cis* to C_6F_5. [a]Proceeds via nucleophilic displacement of Br⁻; all other pathways involve a concerted oxidative addition. See Figures S15-S19 for details and alternative pathways.

coordinate precursor to C–Br activation accessible. The high *trans* influence of the cyclometallated arm is therefore a key factor in promoting reactivity.

The cyclometallated benzoate ligand also plays an important role in dictating the selectivity of the C–C coupling process. The computed structures of the 6-coordinate Ru(IV) species such as intermediate **M** formed upon C–Br activation show a marked distortion away from an octahedral geometry, with a narrowing of the *trans*-C1-Ru-C2 bond that pushes one of the d orbitals up in energy (see Figure 12).[27] This distortion will tend to favor a low spin d^4 configuration, whereas geometries computed in the triplet state (which are often energetically competitive for these Ru(IV) species[28]) exhibit more regular pseudo-octahedral structures.
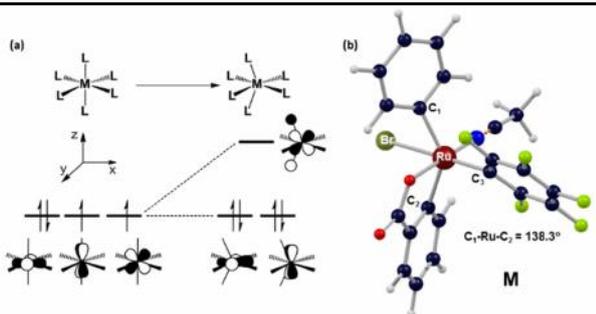

Figure 12. (a) Changes in the relative energies of the metal-based $d\pi$ orbitals and preferred spin state upon narrowing one *trans*-L-M-L angle in d^4 ML_6 complexes. (b) Computed geometry of intermediate **M** highlighting the reduced *trans*-C_1-Ru-C_2 angle.

Distortion of the singlet is most favorable when strong -donors adopt a mutually *trans* arrangement and so the most stable isomers of Ru(IV) species **M** feature the three strongly donating aryl ligands in a *mer* configuration. One of these, **M(ii)**, has Ph *trans* to C_6F_5 and is actually more stable than **M** itself (see Figure 13); moreover C–C coupling with the benzoate ligand in **M(ii)** proceeds through a lower transition state, **$TS_{M(ii)-N(ii)}$** (+11.76 kcal/mol), than that for Ph–C_6F_5 coupling via **TS_{M-N}** (+14.38 kcal/mol). The fact that benzoate–Ph coupling is *not* observed is due to **M(ii)** being kinetically inaccessible, either through C–Br activation at **L(ii)** (via **$TS_{L(ii)-M(ii)}$**, +27.63 kcal/mol) or through isomerization of **M**. The lowest energy isomerization pathway involves Br^- loss to form the neutral trigonal bipyramidal intermediate **$I_{M-M(ii)}$** followed by Br^- re-association to give **M(ii)**; this second step involves transition state **$TS_{M-M(ii)2}$** which, at 17.63 kcal/mol, is > 3 kcal/mol higher than **TS_{M-N}** at 14.38 kcal/mol. Benzoate–C_6F_5 coupling from either **M** or **M(ii)** is also significantly less accessible (see Figure S20). More generally, for the systems in Figure 11 that lack a cyclometallated ligand, C–Br activation is computed to be more accessible when the Ph ligand moves *trans* to C_6F_5. The presence of the cyclometallated benzoate therefore
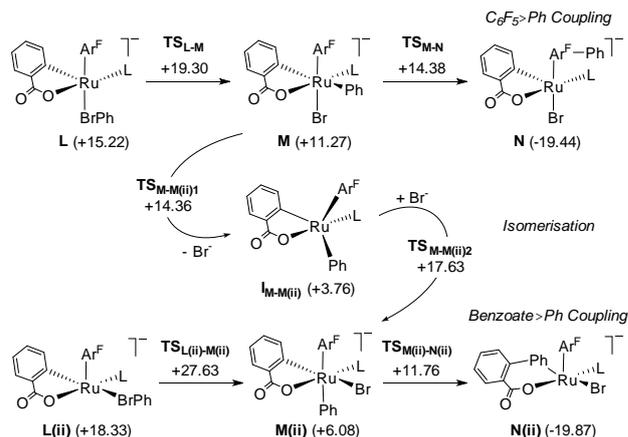

Figure 13. Key stationary points (kcal/mol) for the competition between C_6F_5–Ph coupling via intermediate **M** and benzoate–Ph coupling via intermediate **M(ii)** (L = MeCN, $Ar^F = C_6F_5$).

promotes the formation of a Ru(IV) intermediate where the Ph and C_6F_5 can be mutually cis, thus facilitating the observed selectivity of the subsequent C–C coupling.

The computed data highlight how a C–H functionalization process can be promoted through use of a base additive such as $(NMe_4)OC(CF_3)_3$, and how a subtle perturbation of a C–H activation pre-equilibrium step can have a significant effect on the overall reaction efficiency. Group 1 carbonate salts, M_2CO_3, have often been proposed as proton sinks in direct arylation reactions[29] and the choice of the Group 1 M^+ cation can significantly impact the end result when expressed as a reaction yield. The results here highlight how such variations can result from small changes in the efficiency of these processes that could reflect, for example, changes in additive concentration due to varying solubilities in organic reaction media.

3. CONCLUSIONS

A detailed experimental and *in silico* mechanistic investigation allowed the elucidation of the role of the benzoate salt in promoting aryl halide oxidative addition in the Ru(II)-catalyzed C–H arylation of fluoroarenes. The inability of 2,6-disubstituted benzoate sources to trigger the desired arylation event, along with D/H scrambling and kinetic isotope effect experiments, supported the hypothesis for the requirement of a cyclometallation step of the benzoate salt. Thus, the resulting highly electron-rich anionic Ru(II) intermediate rapidly undergoes oxidative addition with the aryl halide to furnish the biaryl product via a selective reductive elimination step. The pre-equilibrium associated with the kinetically relevant benzoate cyclometallation leads to a Jaffé relationship reflecting the influence of the benzoate substituents at multiple distinctive sites in this process. Indeed, simple Hammett plots correlating the electronic perturbation at only one reactive site at the time could not provide a linear free energy relationship that accommodated all the substituents studied.

DFT calculations provide support for a mechanism involving reversible C–H activation and formation of an anionic cyclometallated intermediate. The enhanced lability of this species allows access to a reactive 5-coordinate intermediate capable of C–Br bond cleavage. A kinetic model based on the computed mechanism captures the rate enhancement observed with *p*-substituted benzoates bearing both electron withdraw-

ing and electron donating substituents. The role of a $(NMe_4)OC(CF_3)_3$ additive in promoting reactivity is pinpointed to the deprotonation of the carboxylic acid formed upon cyclometallation that shifts the pre-equilibrium associated with benzoate cyclometallation. This effect is particularly marked for less basic benzoates such as $(NMe_4)(4-CF_3-C_6H_4CO_2)$, the conjugate acids of which will be more readily deprotonated by the $(NMe_4)OC(CF_3)_3$ additive. Both the experimental and computational results highlight the counter-balancing effects of electron-withdrawing groups *meta* to the site of benzoate cyclometallation and electron donating groups *para* to the proton-accepting carboxylate group in promoting reactivity, with the former having the larger influence by a factor of approximately 2.

Finally, this mechanistic breakthrough has important implications on the design of new catalytic systems involving an oxidative addition at Ru(II) centers, which have been significantly underdeveloped due to the lack of knowledge surrounding this fundamental step.

ASSOCIATED CONTENT

Supporting Information. Experimental procedures and characterization data are available free of charge via the Internet at http://pubs.acs.org.

AUTHOR INFORMATION

Corresponding Author

*igor.larrosa@manchester.ac.uk
*s.a.macgregor@hw.ac.uk

Notes

The authors declare no competing financial interests.

ACKNOWLEDGMENT

REFERENCES

(1) (a) Zahn, A.; Brotschi, C.; Leumann, C. J. *Chem. Eur. J.* **2005**, *11*, 2125–2129. (b) DiMagno, S. G.; H. Sun, *Curr. Top. Med. Chem.* **2006**, *6*, 1473–1482. (c) Purser, S.; Moore, P. R.; Swallow, S.; Gouverneur, V. *Chem. Soc. Rev.* **2008**, *37*, 320–330. (d) Liang, T.; Neumann, C. N.; Ritter, T. *Angew. Chem., Int. Ed.* **2013**, *52*, 8214–8264. (e) Selby, T. P.; Bereznak, J. F.; Bisaha, J. J.; Ding, A. X.; Gopalsamuthiram, V.; Hanagan, M. A.; Long, J. K.; Taggi, A. E. Fungicidal substituted azoles. U.S. Patent WO 2009137651 A8, 2009. (f) Gregory, V.; Taggi, A. E. Fungicidal Mixtures. U.S. Patent WO 2011056463 A2, 2011. (g) G. M.; Naso, F.; Ragni, R. *Chem. Commun.* **2007**, 1003–1022. (h) Tang, M. L.; Reichardt, A. D.; Miyaki, N.; Stoltenberg, R. M.; Bao, Z. *J. Am. Chem. Soc.* **2008**, *130*, 6064–6065. (i) Wang, Y.; Watson, M. D. *J. Am. Chem. Soc.* **2006**, *128*, 2536–2537. (j) Tsuzuki, T.; Shirasawa, N.; Suzuki, T.; Tokito, S. *Adv. Mater.* **2003**, *15*, 1455–1458. (k) Weck, M.; Dunn, A. R.; Matsumoto, K.; Coates, G. W.; Lobkovsky, E. B.; Grubbs, R. H. *Angew. Chem., Int. Ed.* **1999**, *38*, 2741–2745. (i) Nitschke, J. R.; Tilley, T. D. *J. Am. Chem. Soc.* **2001**, *123*, 10183–10190. (l) Kitamura, T.; Wada, Y.; Yanagida, S. *J. Fluorine Chem.* **2000**, *105*, 305–311. (m) Sakamoto, Y.; Suzuki, T.; Miura, A.; Fujikawa, H.; Tokito, S.; Taga, Y. *J. Am. Chem. Soc.* **2000**, *122*, 1832–1833.

(2) (a) DePasquale, R. J.; Tamborski, C. *J. Org. Chem.* **1969**, *34*, 1736–1740. (b) Coe, P. L.; Pearl, G. M. *J. Organomet. Chem.* **1971**, *31*, 55–57. (c) Frohn, H.-J.; Adonin, N. Y.; Bardin, V. V.; Starichenko, V. F. *J. Fluorine Chem.* **2002**, *117*, 115–120. (d) Korenaga, T.; Kosaki, T.; Fukumura, R.; Ema, T.; Sakai, T. *Org. Lett.* **2005**, *7*, 4915–4917. (e) Shang, R.; Fu, Y.; Wang, Y.; Xu, Q.; Yu, H.-Z.; Liu, L. *Angew. Chem., Int. Ed.* **2009**, *48*, 9350–9354. (f) Shang, R.; Xu, Q.; Jiang, Y.-Y.; Wang, Y.; Liu, L. *Org. Lett.* **2010**, *12*, 1000–1003. (g) Kinzel, T.; Zhang, Y.; Buchwald, S. L. *J. Am. Chem. Soc.* **2010**, *132*, 14073–14075.

(3) Representative reviews on C–H activation: (a) Alberico, D.; Scott, M. E.; Lautens, M. *Chem. Rev.* **2007**, *107*, 174–238. (b) Ackermann, L.; Vicente, R.; Kapdi, A. R. *Angew. Chem., Int. Ed.* **2009**, *48*, 9792–9826. (c) Gutekunst, W. R.; Baran, P. S. *Chem. Soc. Rev.* **2010**, *40*, 1976–1991. (d) Lyons, T. W.; Sanford, M. S. *Chem. Rev.* **2010**, *110*, 1147–1169. (e) Boorman, T. C.; Larrosa, I. *Chem. Soc. Rev.* **2011**, *40*, 1910–1925. (f) Wencel-Delord, J.; Droge, T.; Liu, F.; Glorius, F. *Chem. Soc. Rev.* **2011**, *40*, 4740–4761. (g) Arockiam, P. B.; Bruneau, C.; Dixneuf, P .H. *Chem. Rev.* **2012**, *112*, 5879–5918. (h) Engle, K. M.; Mei, T.-S.; Wasa, M.; Yu, J.-Q. *Acc. Chem. Res.* **2012**, *45*, 788–802. (i) Juliá-Hernández, F.; Simonetti, M.; Larrosa, I. *Angew. Chem., Int. Ed.* **2013**, *52*, 11458–11460. (j) Girard, S. A.; Knauber, T.; Li, C. J. *Angew. Chem., Int. Ed.* **2014**, *53*, 74–100. (k) Kakiuchi, F.; Kochi, T.; Murai, S. *Synlett* **2014**, *25*, 2390–2414. (l) Tani, S.; Uehara, T. N.; Yamaguchi, J.; Itami, K. *Chem. Sci.* **2014**, *5*, 123–135. (m) Zhang, X.-S.; Chen, K.; Shi, Z. *Chem. Sci.* **2014**, *5*, 2146–2159. (n) Yang, J. *Org. Biomol. Chem.* **2015**, *13*, 1930–1941. (o) Dey, A.; Agasti, S.; Maiti, D. *Org. Biomol. Chem.* **2016**, *14*, 5440–545. (p) Dey, A.; Maity, S.; Maiti, D. *Chem. Commun.* **2016**, *52*, 12398–12414. (q) Simonetti, M.; Cannas, D. M.; Larrosa, I. In *Advances in Organometallic Chemistry*; Perez, P. J., Ed.; Elsevier: Amsterdam, 2017; Vol. 67, pp 299–399.

(4) (a) Lafrance, M.; Rowley, C. N.; Woo, T. K.; Fagnou, K. *J. Am. Chem. Soc.* **2006**, *128*, 8754–8756. (b) Lafrance, M.; Shore, D.; Fagnou, K. *Org. Lett.* **2006***, 22*, 5097–5100. (c) René. O.; Fagnou, K. *Org. Lett.* **2010**, *12*, 2116–2119. (d) Gorelsky, S. I. *Coord. Chem. Rev.* **2013**, *257*, 153–164. (e) Wei, Y.; Kan, J.; Wang, M.; Su, W.; Hong, M. *Org. Lett.* **2009**, *11*, 3346–3349. (f) Wei, Y.; Su, W. *J. Am. Chem. Soc.* **2010**, *132*, 16377–16379. (g) Li, H.; Liu, J.; Sun C.-L.; Li, B.-J.; Shi, Z. *Org. Lett.* **2011**, *13*, 276–279.

(5) (a) Do, H.-Q.; Daugulis, O. *J. Am. Chem. Soc.* **2008**, *130*, 1128–1129. (b) Do, H.-Q.; Khan, R. M. K.; Daugulis, O. *J. Am. Chem. Soc.* **2008**, *130*, 15185–15192. (c) Do, H.-Q.; Daugulis, O. *Chem. Commun.* **2009**, 6433–6435. (d) Do, H.-Q.; Daugulis, O. *J. Am. Chem. Soc.* **2009**, *131*, 17052–17053. (e) Do, H.-Q.; Daugulis, O. *J. Am. Chem. Soc.* **2011**, *133*, 13577–13586.

(6) (a) Lu, P.; Boorman, T. C.; Slawin, A. M. Z.; Larrosa, I. *J. Am. Chem. Soc.* **2010**, *132*, 5580–5581. (b) Ahlsten, N.; Perry, G. J. P.; Cambeiro, X. C.; Boorman, T. C.; Larrosa, I. *Catal. Sci. Technol.* **2013**, *3*, 2892–2897. (c) Cambeiro, X. C.; Boorman, T. C.; Lu, P.; Larrosa, I. *Angew. Chem., Int. Ed.* **2013**, *52*, 1781–1784. (d) Cambeiro, X. C.; Ahlsten, N.; Larrosa, I. *J. Am. Chem. Soc.* **2015**, *137*, 15636–15639.

(7) Simonetti, M.; Perry, G. J. P.; Cambeiro, X. C.; Juliá-Hernández, F.; Arokianathar, J. N.; Larrosa, I. *J. Am. Chem. Soc.* **2016**, *138*, 3596–3606.

(8) Simonetti, M.; Cannas, D. M.; Just-Baringo, X.; Vitorica-Yrezabal, I. J.; Larrosa, I. *Nat. Chem.* **2018**, *10*, 724–731.

(9) (a) Ackermann, L. *Acc. Chem. Res.* **2014**, *47*, 281–295. (b) De Sarkar, S.; Liu, W.; Kozhushkov, S. I.; Ackermann, L. *Adv. Synth. Catal.* **2014**, *356*, 1461–1479. (c) Simonetti, M.; Larrosa, I. *Nat. Chem.* **2016**, *8*, 1086–1088.

(10) (a) Simonetti, M.; Cannas, D. M.; Panigrahi, A.; Kujawa, S.; Kryjewski M.; Xie, P.; Larrosa, I. *Chem. Eur. J.* **2017**, *23*, 549–553. (b) Huang, L.; Weix, D. J. *Org. Lett.* **2016**, *18*, 5432–5435. (c) Biafora, A.; Krause, T.; Hackenberger, D.; Belitz, F.; Gooßen, L. J. *Angew. Chem., Int. Ed.* **2016**, *55*, 14752–14755. (d) Mei, R.; Zhu, C.; Ackermann, L. *Chem. Commun.* **2016**, *52*, 13171–13174.

(11) (a) Ackermann, L. *Acc. Chem. Res.* **2014**, *47*, 281–295. (b) Ackermann, L.; Vicente, R.; Althammer, A. *Org. Lett.* **2008**, *10*, 2299–2302. (c) Ackermann, L.; Vicente, R.; Potukuchi, H. K.; Pirovano, V. *Org. Lett.* **2010**, *12*, 5032–5035. (d) Ackermann, L. *Chem. Rev.* **2011**, *111*, 1315–1345. (d) Ferrer Flegeau, E.; Bruneau, C.;

Dixneuf, P. H.; Jutand, A. *J. Am. Chem. Soc.* **2011**, *133*, 10161–10170.

(12) When (2,6-Me-C$_6$H$_3$CO$_2$)(NMe$_4$), (2,6-F-C$_6$H$_3$CO$_2$)(NMe$_4$) and (2,6-OMe-C$_6$H$_3$CO$_2$)(NMe$_4$) were tested in the presence of added (NMe$_4$)OC(CF$_3$)$_3$, no cross-coupled product was detected.

(13) In light of the reversibility of steps **I-IV** (Scheme 3), the observed KIE of 1.36 could also be associated with the C–H activation step of C$_6$F$_5$H/D, which is likely being generated *in situ* during via protono/deuterolysis of **Ru1c** with concomitant release of Ru(C$_6$H$_5$CO$_2$)$_x$(*t*-BuCN)$_y$ species. In order to rule this hypothesis out, we pre-incubated C$_6$F$_5$H (1 equiv), [Ru(*t*-BuCN)$_6$](BF$_4$)$_2$ (1 equiv), (C$_6$H$_5$CO$_2$)(NMe$_4$) (2.5 equiv) and (NMe$_4$)OC(CF$_3$)$_3$ (3.0 equiv) in *t*-BuCN (0.1 M) at 90 °C for 20 min. After this time, 5-bromo-*m*-xylene (2 equiv) was added and then the reaction was stopped after 18 min, which correspond to the last kinetic data point taken into consideration for calculating the KIE (**3cb**$_{(18 min)}$= 11.65%). The reaction was analysed by calibrated GC-FID revealing only traces of biaryl product (**3cb**$_{(18 min)}$= 0.02%). As this experiment was carried out mimicking the extreme case scenario in which the equilibrium **I-IV** is totally shifted towards **I** under the reaction conditions used for the determining the KIE, it further validates that the value of 1.36 is exclusively associated with the cyclometallation step of the benzoate (see SI, section 3).

(14) The $_m$ and $_p$ values were taken from: Hansch, C.; Leo, A.; Taft, R. W. *Chem. Rev.* **1991**, *91*, 165–195.

(15) For leading discussions of the correlation of the rate of electrophilic substitution reaction with Hammett equation, see ref. 12 and: (a) Hammett, L. P. *J. Am. Chem. Soc.* **1937**, *59*, 96–109. (b) Jaffé, H. H. *Chem. Rev.* **1953**, *53*, 191–261. (c) Brown, H. C.; Okamoto, Y. *J. Am. Chem. Soc.* **1957**, *79*, 1913–1917. (c) Brown, H. C.; Okamoto, Y. *J. Am. Chem. Soc.* **1958**, *80*, 4979–4987. (d) Stock, L. M.; Brown, H. C. *Adv. Phys. Org. Chem.* **1963**, *1*, 35–154. (e) Charton, M. *J. Org. Chem.* **1969**, *34*, 278–285. (f) Gawley, R. E. *J. Org. Chem.* **1981**, *46*, 4595–4607. (g) Santiago, C. B.; Milo, A.; Sigman, M. S. *J. Am. Chem. Soc.* **2016**, *138*, 13424–13430.

(16) (a) Swansburg, S.; Buncel, E.; Lemieux, R. P. *J. Am. Chem. Soc.* **2000**, *122*, 6594–6600. (b) Zdilla, M. J.; Dexheimer, J. L.; Abu-Omar, M. M. *J. Am. Chem. Soc.* **2007**, *129*, 11505–11511. (c) Edwards, D. R.; Hleba, Y. B.; Lata, C. J.; Calhoun, L. A.; Crudden, C. M.; *Angew. Chem., Int. Ed.* **2007**, *46*, 7799–7802. (d) Stokes, B. J.; Richert, K. J.; Driver, T. G. *J. Org. Chem.* **2009**, *74*, 6442–6451. (e) Konnick, M. M.; Decharin, N.; Popp, B. V.; Stahl, S. S. *Chem. Sci.* **2011**, *2*, 326–330. (f) Aihara, Y.; Chatani, N. *Chem. Sci.* **2013**, *4*, 664–670. (g) Neu, H. M.; Yang, T.; Baglia, R. A.; Yosca, T. H.; Green, M. T.; Quesne, M. G.; de Visser, S. P.; Goldberg, D. P. *J. Am. Chem. Soc.* **2014**, *136*, 13845–13852. (h) Kalutharage, N; Yi, C. S. *J. Am. Chem. Soc.* **2015**, *137*, 11105–11114.

(17) (a) Jaffé, H. H. *J. Am. Chem. Soc.* **1954**, *76*, 4261–4264. (b) Bromilow, R. H.; Kirby, A. J. *J. Chem. Soc. Perkin Trans. 2* **1972**, 149–155. (c) Hopkins, A. R.; Green, A. L.; Williams, A. *J. Chem. Soc. Perkin Trans. 2* **1983**, 1279–1283. (d) Craze, G.-A.; Kirby, A. J. *J. Chem. Soc. Perkin Trans. 2* **1974**, 61–66. (f) Barber, S. E.; Dean, K. E. S.; Kirby, A. J. *Can. J. Chem.* **1999**, *77*, 792–801, (e) Greig, I. R.; Kirby, A. J. *J. Phys. Org. Chem.* **2004**, *17*, 498–506. (f) Edwards, D. R.; Neverov, A. A; Brown, R. S. *J. Am. Chem Soc.* **2009**, *131*, 368–377. (g) Jensen, K. H.; Webb, J. D.; Sigman, M. S. *J. Am. Chem Soc.* **2010**, *132*, 17471–17482

(18) Davies, D. L.; Macgregor, S. A.; McMullin, C. L., *Chem. Rev.* **2017** *117*, 8649–8709.

(19) A more stable *mer*-isomer is computed at +7.29 kcal/mol, but the isomerization pathway to form this species involves a transition state at +24.05 kcal/mol and, as such, is less accessible than the onward PhBr activation via **TS(IV'-V')**. See Figure S14, ESI.

(20) A triplet transition state for PhBr activation was located at +61.41 kcal/mol and the triplet state was also assessed for all isomers of the Ru(II) precursor **Int(IV'-V')** and found to be very high in energy. Reaction via a triplet spin state can therefore be ruled out (see Figures S5 and S7, ESI).

(21) **TS$_{K-L}$** is in fact slightly higher than the C–Br activation transition state **TS$_{L-M}$** for all three benzoates. Based on this ΔG$_{span}$ is 25.57 kcal/mol, 21.84 kcal/mol and 24.02 kcalmol for R = H, NMe$_2$ and CF$_3$ respectively, and thus follows the same trend as the data in the table.

(22) (a) Gorelsky, S. I.; Lapointe, D.; Fagnou, K., *J. Am. Chem. Soc.* **2008,** *130*, 10848–10849. (b) Gorelsky, S. I.; Lapointe, D.; Fagnou, K., *J. Org. Chem.* **2012**, *77*, 658–668.

(23) For a recent example where the net effect of arene *para* substituents is the result of two counter-balancing effects see: Frasco, D. A.; Mukherjee, S.; Sommer, R. G.; Perry, C. M.; Lambic, N. K.; Abboud, K. A.; Jakubikova, E.; Ison, E. A. *Organometallics* **2016**, *35*, 2435–2445.

(24) (a) Eisenstein, O.; Milani, J.; Perutz, R. N. *Chem. Rev.* **2017**, *117*, 8710–8753. (b) Clot, E.; Eisenstein, O.; Jasim, N.; Macgregor, S. A.; McGrady, J. E.; Perutz, R. N. *Acc. Chem. Res.* **2011**, *44*, 333–348.

(25) (a) Evans, M. E.; Li, T.; Vetter, A. J.; Rieth, R. D.; Jones, W. D. *J. Org. Chem.* **2009**, *74*, 6907–6914. (b) Jones, W. D. *J. Inorg. Chem.* **2005**, *44*, 4475–4484.

(26) (a) The higher energy of the Ph–Br activation transition state at [Ru(C$_6$F$_5$)(MeCN)(κ^1-PhCO$_2$)$_2$(PhBr)]$^-$ compared to [Ru(C$_6$F$_5$)(κ^2-PhCO$_2$)(κ^1-PhCO$_2$)(PhBr)]$^-$ and [Ru(C$_6$F$_5$)(MeCN)$_2$(κ-*C,O*-C$_6$H$_4$CO$_2$)(PhBr)]$^-$ may reflect the geometry imposed on the metal center by the κ^2-PhCO$_2$$^-$ (O-Ru-O= 62°) and cyclometallated (C-Ru-O = 82°) ligands; in comparison the O-Ru-O angle in [Ru(C$_6$F$_5$)(MeCN)(κ^1-PhCO$_2$)$_2$(PhBr)]$^-$ is 90°. A similar bite angle effect is known to promote oxidative addition in d^{10} ML$_2$ species by destabilizing an occupied metal-based dπ orbital.[26b,c] The low symmetry of the current systems causes significant orbital mixing and thus complicates a detailed analysis; however the average energies of the three occupied dπ orbitals in [Ru(C$_6$F$_5$)(κ^2-PhCO$_2$)(κ^1-PhCO$_2$)(PhBr)]$^-$ and [Ru(C$_6$F$_5$)(MeCN)$_2$(κ-*C,O*-C$_6$H$_4$CO$_2$)(PhBr)]$^-$ are 6-7 kcal/mol above those for [Ru(C$_6$F$_5$)(MeCN)(κ^1-PhCO$_2$)$_2$(PhBr)]$^-$, suggesting that a bite angle effect could also contribute to reducing the barrier to Ph–Br activation here. (b) Albright T. A.; Burdett J. K.; Whangbo M. H. *Orbital Interactions in Chemistry*, 2nd edn. Wiley, New York, 2013. (c) Wolters, L. P.; Bickelhaupt, F. M., in *Computational Studies in Organometallic Chemistry*, Macgregor, S. A.; Eisenstein, O., Eds. **2016**, *167*, 139–161.

(27) Hoffmann, R.; Howell, J. M.; Rossi, A. R. J. Am. Chem. Soc. 1976, 98, 2484–2492.

(28) The triplet state of the Ru(II) precursors is always strongly disfavored and so C–Br activation pathways computed on the triplet surface were found to be prohibitively high in energy.

(29) (a) Rousseaux, S.; Gorelsky, S. I.; Chung, B. K. W.; Fagnou, K. *J. Am. Chem. Soc.* **2010**, *132*, 10692–10705. (b) Sun, H.-Y.; Gorelsky, S. I.; Stuart, D. R.; Campeau, L.-C.; Fagnou, K. *J. Org. Chem.* **2010**, *75*, 8180–8189. (c) Zhang, M.; Huang, G. *Chem. Eur. J.* **2016**, *22*, 9356–9365.(d) Sanhueza, I. A.; Wagner, A. M.; Sanford, M. S.; Schoenebeck, F. *Chem. Sci.* **2013**, *4*, 2767–2775.